01,13

Thermodynamic and surface properties of platinum with changes in temperature, pressure, and crystal size

© S.P. Kramynin

Federal State Budget Scientific Institution „Amirkhanov Institute of Physics“ Dagestan Federal Research Center, Russian Academy of Sciences,
Makhachkala, Russia

E-mail: kraminin@mail.ru

Received October 21, 2025
Revised November 10, 2025
Accepted November 12, 2025

Based on the parameters of the Mie–Lennard-Jones pair potential for interatomic interactions for Pt and using the RP model of a nanocrystal, size, temperature, and pressure dependences were obtained for various properties: elastic modulus, coefficient of thermal expansion, surface energy, the derivative of surface energy with respect to temperature, and Poisson's ratio. Calculations of the size dependencies of these properties were performed along two isobars: 0 and 50 GPa. For the first time, the following dependences were obtained for macro- and nanocrystals: pressure dependences of surface energy, pressure and temperature dependences of the derivatives of surface energy with respect to temperature and pressure; pressure and temperature dependences for the product of elastic modulus and thermal expansion coefficient; and the temperature depedence of Poisson's ratio for a nanocrystal.

Keywords: platinum, nanocrystal, size dependences, equation of state, surface energy, poisson's ratio.

DOI: 10.61011/PSS.2025.11.62950.286-25

1. Introduction

Platinum is widely used in scientific and industrial devices thanks to its unique mechanical, thermal and physical and chemical properties. In particular, platinum is heat-resistant and may withstand mechanical loads in aggressive media at very high temperatures for many thousands of hours. Platinum is often used as a high-temperature marker of pressure in the laser heating experiments due to its ability to absorb laser radiation well and absence of structural transitions under significant compressions, and chemical resistance. Platinum is widely used in renewable energy sector, petrochemical industry, automotive industry and pharmaceutical engineering [1].

Platinum is under constant monitoring of the researchers in the field of extremely high pressures. Thus, paper [2] studied the equation of state of platinum at pressures of up to 430 GPa. Such high pressures are of interest not only in the aspect of the solid-state science, but in the study of properties of the substances inside the planets of much larger size than the Earth, for example, gas and ice giants. The authors of paper [3] studied the properties of platinum being one of the most important standard materials in static and dynamic experiments with high pressure, under the conditions of extreme pressures by methods of impact compression in the range of up to 1.1 TPa. Despite the fact that platinum is a widely studied metal, some dependences for the FCC-Pt macrocrystal remain unstudied, both experimentally and even theoretically. For example, baric dependences of BT modulus of elasticity are only presented in the paper by P.I. Dorogokupets [4], baric dependences of thermal expansion coefficient are presented only by two papers [4,5]. For the specific (per unit of surface area) surface energy, the baric dependences are not presented in the literature, therefore, the derivatives of the surface energy by temperature and pressure have not been studied, too. Besides, there are no temperature and baric dependences for the product of $B_T\alpha_p(P)$, often this product is treated as a constant.

Analysis of the platinum nanocrystals at this time is an actively developing topic in the studies of many authors [6–10]. Note that mainly the papers related to the nanocrystals are dedicated to the study of the nanocrystals as such and are less often dedicated to the study of their thermodynamic properties. For example, platinum NC of irregular tetrahexahedral (THH) shape, with the size of around ~ 100 nm, were obtained with high yield by electrochemical treatment of Pt nanospheres applied on glassy carbon [6]. Catalytic activity of THH Pt nanocrystals exceeds the catalytic activity of spherical Pt nanoparticles. NC were used to accelerate electric oxidation of formic acid and ethanol, which are promising alternative types of fuel for straight fuel elements [6]. In paper [7] they studied nucleation and growth of nanocrystals formed by ligand-platinum compounds. Understanding of these processes is necessary for rational design of functional nanocrystals with a clearly defined composition, shape and size for use in catalysis, medicine and nanotechnology. Mechanisms of platinum nanocrystals growth from individual atoms to end crystals in the atomic scale were studied using *in situ* liquid-phase scanning transmission electron microscopy in article [8]. In paper [9] it is stated that the controlled

Comparison of properties of FCC-Pt at $P = 0$ and $T = 300\,\mathrm{K}$, obtained in this paper with literature data

	V_0 ($\mathrm{cm^3/mol}$)	α_p ($10^{-6}\,\mathrm{K^{-1}}$)	B_T (GPa)	$(\partial B_T/\partial P)_T$	Θ (K)	γ
Our results for $N = \infty$	9.0215	25.36	238.09	6.93	249	2.27
Our results for $N = 306$, $f = 1$	8.8699	29.01	208.35	6.93	238	2.27
Literature data	9.094 [2] 9.091 [4] 9.090 [5] 9.0946 [13] 9.1075 [14] 9.0888−9.1254 [15] 9.0783 [16] 8.9657−9.5173 [17] 9.0904 [18] 9.1161 [19] 9.041 [20] 9.090 [21]	26.82 ± 0.15 [15] 19.4 [17] 26.79 [20]	274.1 [2] 276.07 [4] 273.5 [5] 259.7 [13] 260.10−279.10 [14] 274.4 [15] 274 [16] 251.21−310.24 [17] 275.3 [18] 276.4 [19] 273 [21]	5.128 [2] 5.30 [4] 4.70 [5] 5.839 [13] 5.10−5.8 [14] 5.66 [15] 5.5 [16] 5.207 [17] 4.78 [18] 5.12 [19] 4.8 [21]	230 [5] 230 [19] 230 [21]	2.802 [4] 2.75 [5] 2.64 [15] 2.18 [17] 2.63 [19] 2.69 [21]

growth of Pt nanoparticles, the shape of which is far from the equilibrium one, with the possibility to select the size is critical for the study of their unique physical and chemical properties. Using coherent diffraction Bragg visualization, in paper [10] they observed the abnormal sliding plane {110} in two submicron Pt crystals grown by absolutely different methods and having absolutely different morphology. Using the specified method, the authors of paper [10] studied the plasticity and unusual behavior of defects at the nanoscale. However, the dependence of thermoelastic properties on the size and shape of Pt nanocrystal in the literature is hardly understood. There are only articles that study the size-dependent fusioning temperature of Pt nanocrystal at zero pressure.

Based on the absence of the above dependences for nanocrystals, in our paper we use the same positions, based on the formalism [11] and the RP-model of nanocrystal from [12] to calculate for the first time the baric dependences of surface energy for the FCC-Pt macro- and nanocrystal, and the charts were also produced for baric and temperature dependences of derivatives of surface energy by temperature and pressure. The evolution of baric dependences B_T and α_p is shown in a transition from a macro- to a nanocrystal. For the first time the baric and temperature dependences are obtained for the product of $B_T\alpha_p$, both for the FCC-Pt macro- and the nanocrystal. It is shown that $B_T\alpha_p$ is not a constant and may be accepted as such only under certain $P-T$ conditions. Size dependence are presented along three different isotherms for the modulus of elasticity B_T, volume thermal expansion coefficient α_p, and also for the specific surface energy σ. For the first time the Poison's ratio was calculated for Pt nanocrystal.

2. Calculation method

To calculate the properties of the face-centered crystal (FCC) of Pt crystal, let us imagine a pairwise interatomic interaction in the form of Mie−Lennard-Jones potential [11]:

$$\varphi(r) = \frac{D}{(b-a)}\left[s\left(\frac{r_0}{r}\right)^b - b\left(\frac{r_0}{r}\right)^a\right], \qquad (1)$$

where D and r_o — depth and coordinate of the minimum potential, $b > a > 1$ — parameters.

Thermodynamic properties were calculated on the basis of formalism from [11]. To calculate the properties of FCC platinum, the following parameters were used: atomic weight $m(\mathrm{Pt}) = 195.08\,\mathrm{Da}$; $k_n(\infty) = 12$ — first coordination number in the macrocrystal and $k_p = 0.7405$ — packing index of FCC structure. Parameters of the potential (1) were defined in paper [11] and are accordingly the following:

$$r_o = 2.7675 \cdot 10^{-10}\,\mathrm{m},\ D/k_B = 11400.7\,\mathrm{K},$$

$$a = 3.05,\ b = 11.65. \qquad (2)$$

The table presents the results of calculations of the following thermodynamic properties of platinum at $P = 0$ and $T = 300\,\mathrm{K}$: V_0 ($\mathrm{cm^3/mol}$) — molar volume; $B_T = -v(\partial P/\partial v)_T$ (GPa) — modulus of elasticity, v — specific volume per number of particles; $\alpha_p = C_v/V \cdot B_T$ ($10^{-6}\,\mathrm{K^{-1}}$) — volume thermal expansion coefficient, C_v — isochoric heat capacity, V — volume; $(\partial B_T/\partial P)_T$ — derivative of modulus of elasticity by pressure at $T = 300\,\mathrm{K}$; Θ (K) — Debye temperature; γ — first Gruneisen parameter. Besides, the table also compares the obtained results with the literature data from more than ten sources. It should be noted that the model [11] bundled with

the RP-model [12] makes it possible to calculate the size dependences of nanocrystal properties.

As you can see from the comparison, the calculated values match well the literature data. Good match between our data and the literature data makes it possible to use the potential (1) and the calculation method from [11] to study the baric, temperature, and also size dependences of thermoelastic properties of FCC-Pt.

3. Results

Figure 1 shows the isotherms of the FCC-Pt equation of state. Pressure is given in GPa, the specific volume, in Figure 1, *a* — in $cm^3/mol = 10^{-6}\ m^3/mol$, and in Figure 1, *b* — in relative units. The solid lines mark our calculations of the isotherms 300, 1300 and 1900 K. The dashed lines show the results of the calculations of the 300 K isotherms from [18]. The squares show the isotherm 300 K, the circles — 1300 K, triangles — 1900 K from paper [5]. The dash-dotted lines present the data for the isotherm 300 K from article [13]. As you can see from Figure 1, our data matches well the literature data.

Figure 2 shows the baric dependences of the modulus of elasticity (B_T in GPa, on the right) and the thermal

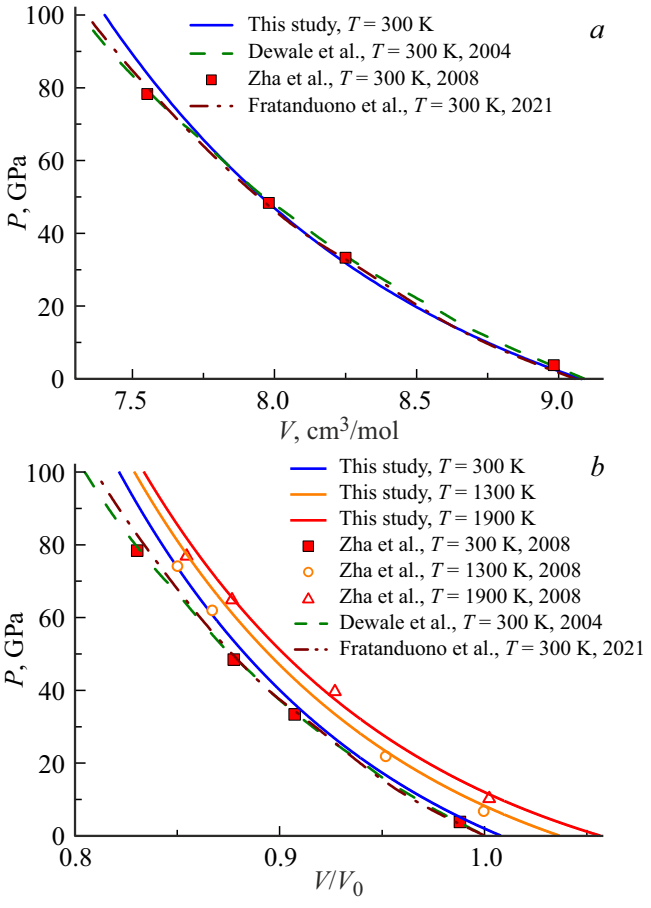

Figure 1. Isotherms of the equation of state for FCC-platinum macrocrystal.

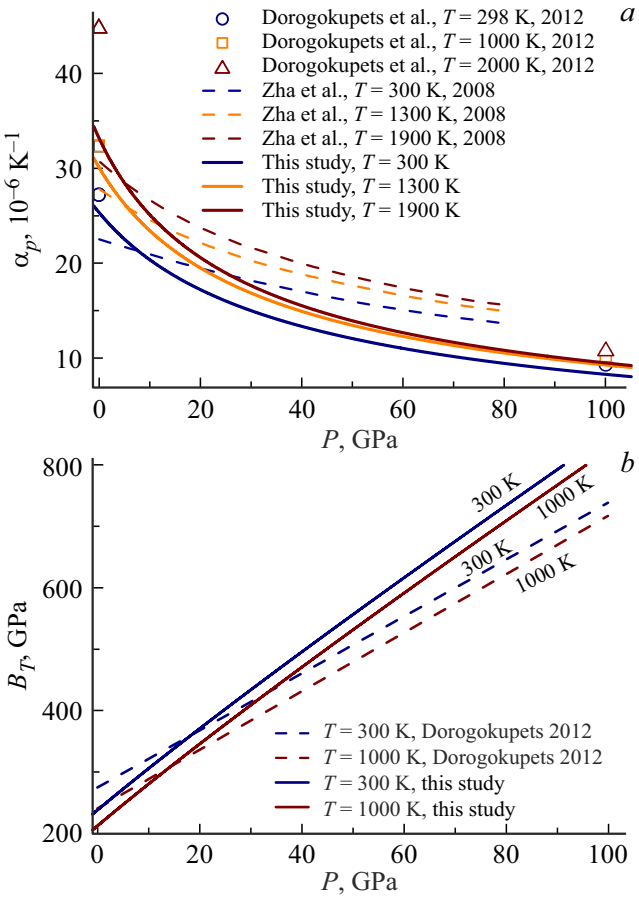

Figure 2. Baric dependence of thermal expansion coefficient (on the left) and modulus of elasticity (on the right) for FCC platinum.

expansion coefficient (α_p in 10^{-6} 1/K, on the left) FCC-Pt. The solid lines on the left show our calculations of the isotherms 300, 1300, 1900 K, the solid lines on the right show our calculations for the isotherms 300 and 1000 K. The left chart uses open circles, squares and triangles to show the calculations of isotherms 298, 1000 and 2000 K for α_p (in the left chart) from paper [4]. The dashed lines in the left chart show the data for α_p isotherms 298, 1300, 1900 K from [5]. The dashed lines in the right chart show the data for B_T isotherms 298, 1000 from [4].

The analysis shown in Figure 1 and 2, demonstrates good agreement between the results of our calculations and the data obtained by other authors in [4,5,13,18]. In connection therewith, the specified method with the parameters of the potential (2) was applied by us for the calculation of baric, temperature and size dependences of the FCC-Pt macro- and nanocrystal.

In Figure 3 two bottom lines — isotherms $T = 300$ K, two top lines — isotherms T=1000 K. The solid lines — calculations for the Nb macrocrystal, the dotted lines — for the nanocrystal from $N = 306$ atoms and $f = 1$, hereinafter f — the shape parameter. Based on the RP-model, let us assume that nanocrystal with free Gibbs surface has the form of a rectangular parallelepiped with a square base,

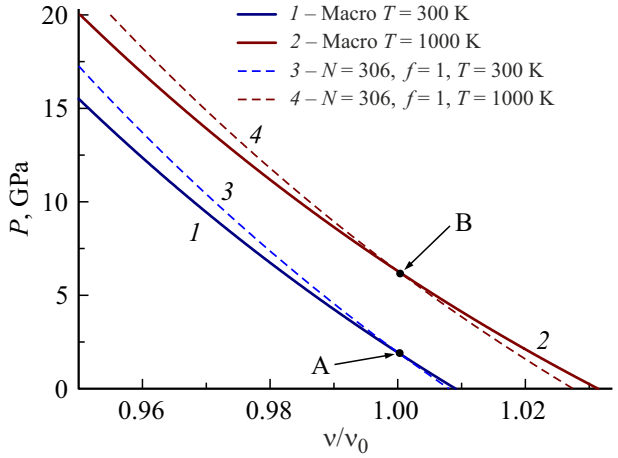

Figure 3. Equation of state for macro- and nanocrystals of FCC-platinum.

faceted with (100) type faces. The value $f = N_{ps}/N_{po}$ is a shape parameter, which is determined by the ratio of the number of atoms on the side edge N_{ps} to the number of atoms on the base edge N_{ps}. For a rod-like shape $f > 1$, for a cube $f = 1$, for a plate-shaped nanocrystal $f < 1$. The number of atoms in nanocrystal is equal to: $N = f(N_{po})^3/\alpha$, varies within: $23 \le N \le \infty$, where$\alpha = \pi/(6k_p)$ — parameter of the structure. As the shape deviates from the energetically optimal one, i. e. from $f = 1$, all size dependences for the nanocrystal become more evident [11,22].

The magnitude of pressure rise in a nanocrystal is lower than the one in a macrocrystal, indicating a reduction in the modulus of elasticity as the size decreases. The chart contains the points where the isotherms of the equation of state of the macro- and nanocrystals intersect with the coordinates:

$$P_A = 1.87\,\text{GPa},\ \ (v/v_o)_A = 1.0003,\ \ T = 300\,\text{K};$$

$$P_B = 6.16\,\text{GPa},\ \ (v/v_o)_B = 1.0005,\ \ T = 1000\,\text{K}.$$

In these points the pressure does not depend on the size (N) at this temperature and shape of the nanocrystal.

The comparison of isomorphic $f = 1$ isothermal baric dependences of the compression modulus $B_T = -v(\partial P/\partial v)_T$, for the macro- and nanocrystal of platinum at $N = 306$ and $f = 1$ is shown in Figure 4. The lines *1* and *2* are calculations for the macrocrystal along isotherms 300 and 1000 K, the lines *3* and *4* are the calculations for the nanocrystal at $N = 83$ and $f = 1$ along the isotherms 300 and 1000 K. You can see that the value B_T for the nanocrystal is always lower than for the macrocrystal at the same temperature. As it is clearly obvious from the obtained results, the modulus of elasticity $B_T(N)$ decreases at the isothermal-isomorphic reduction of the number of atoms N.

The baric dependences of the derivative of the modulus of elasticity $(\partial B_T/\partial P)_T$ for the FCC-Pt macro- and nanocrystal at $N = 306$ and $f = 1$ are shown in Figure 5. The solid lines are calculations for the macrocrystal along isotherms $T = 300$ and 1000 K, the dashed lines are the calculations for the nanocrystal at $N = 306$ and $f = 1$ along the isotherms 300 and 1000 K. You can see that the dependence contains the points with the coordinates:

$$P_{A1} = 0.09\,\text{GPa};\ ((\partial B_T/\partial P)_T)_{A1} = 6.93 \text{ for } T = 300\,\text{K},$$

$$P_{A2} = 1.76\,\text{GPa};\ ((\partial B_T/\partial P)_T)_{A2} = 6.93 \text{ for } T = 1000\,\text{K},$$

where $(\partial B_T/\partial P)_T$ does not depend on N and on f for this temperature.

There are also the following points with the coordinates:

$$P_{B1} = 33.46\,\text{GPa};\ ((\partial B_T/\partial P)_T)_{B1} = 6.14 \text{ for } N = 306,$$

$$P_{B2} = 37.89\,\text{GPa};\ ((\partial B_T/\partial P)_T)_{B2} = 6.14 \text{ for } N = \infty,$$

where $(\partial B_T/\partial P)_T$ does not depend on the temperature at this N.

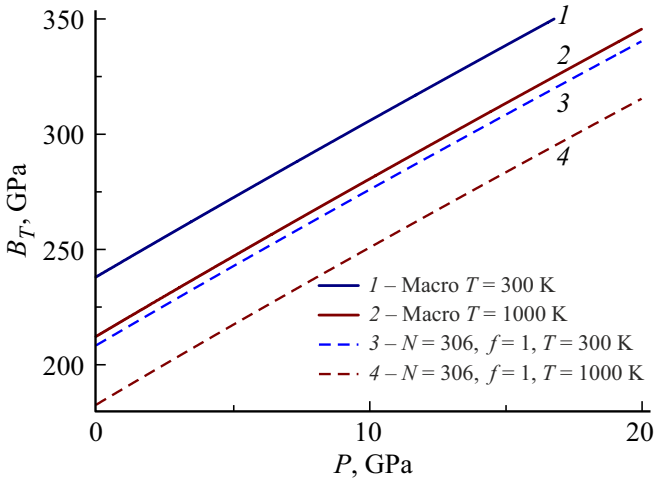

Figure 4. Baric dependences of the compression modulus B_T for macro- and nanocrystals of platinum.

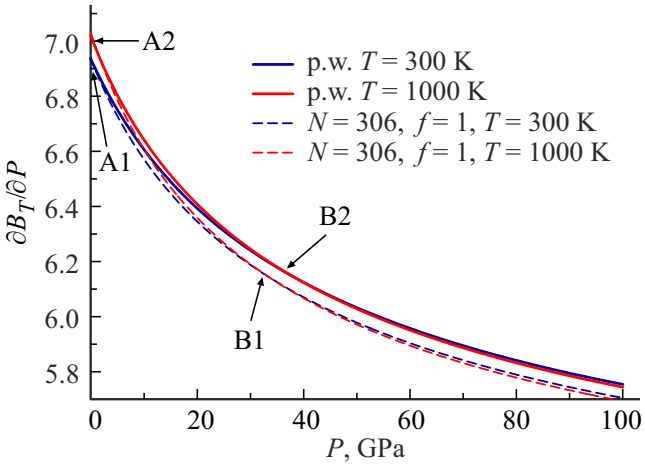

Figure 5. Baric dependences of the derivative of the compression modulus $(\partial B_T/\partial P)_T$ for macro- and nanocrystals of Pt.

Figure 6 shows isomorphic ($f = 1$ and $f = 20$) isobaric ($P = 0$) size dependences of the modulus of elasticity of platinum along three isotherms. Squares, circles and triangles — isotherms 100, 300 and 1000 K, accordingly. The solid lines show the calculations for the shape parameter $f = 1$, the dashed ones — for $f = 20$. You can see that as the size decreases, the value B_T decreases. Besides, these dependences illustrate the statement that whenever the shape factor value moves away from the energetically favorable one ($f = 1$, corresponding to the cubic shape for the RP-model) — the size dependences strengthen, i.e. at one and the same quantity of atoms and at the same temperature the modulus of elasticity will be lower for the system having higher deviation from $f = 1$. You can see that as the number of atoms decreases, at a certain N, the dependences $B_T = f(\lg(N))$ break. It is due to the fact that at the lower number of atoms a configuration with the constant shape factor is not possible. It should be noted that the specified features are common for other size dependences presented in this paper.

Figure 7 shows the comparison of the baric dependences of the volume thermal expansion coefficient: $\alpha_p(P) = (1/v)(\partial v/\partial T)_P$, for the FCC-platinum macro- and nanocrystal at $N = 306$ and $f = 1$. The solid lines are calculations for the macrocrystal along isotherms 300 and 1000 K, the dashed lines are the calculations for the nanocrystal at $N = 306$ and $f = 1$ along the isotherms 300 and 1000 K.

You can see that at this P the dependences for the nanocrystal are higher than for the macrocrystal, which is due to the contribution of the surface, where the atoms oscillate with higher amplitude.

Figure 8 shows the comparison of the baric dependences of the derivative $(\partial\alpha_p/\partial P)_T$ for the macro- and nanocrystal of platinum at $N = 306$ and $f = 1$. The solid lines are calculations for the macrocrystal along isotherms $T = 300$ and 1000 K, the dotted lines are the calculations for the nanocrystal at $N = 306$ and $f = 1$ along the isotherms $T = 300$ and 1000 K. You can see that the dependences $(\partial\alpha_p/\partial P)_T$ from P for the nanocrystal are lower than for the macrocrystal.

Figure 9 shows Isomorphic ($f = 1$ and $f = 20$) isobaric ($P = 0$) size dependences of the volume thermal expansion coefficient $\alpha_p(\lg(N))$ for three isotherms. Squares, circles and triangles — isotherms $T = 100, 300$ and 1000 K, accordingly. The solid lines show the calculations for the shape parameter $f = 1$, the dashed ones — for $f = 20$. You can see that as the size decreases, the value α_p increases, and as the temperature increases, the dependence of function α_p on the size (i.e. on N) strengthens, it is shown that the size dependences strengthen for the shape that drastically differs from the cubic one ($f = 20$).

Figure 10 shows the dependence of the product of modulus of elasticity and the thermal expansion coefficient: $B_T\alpha_p(P) = (\partial P/\partial T)_v$, for the macro- and nanocrystal of Pt

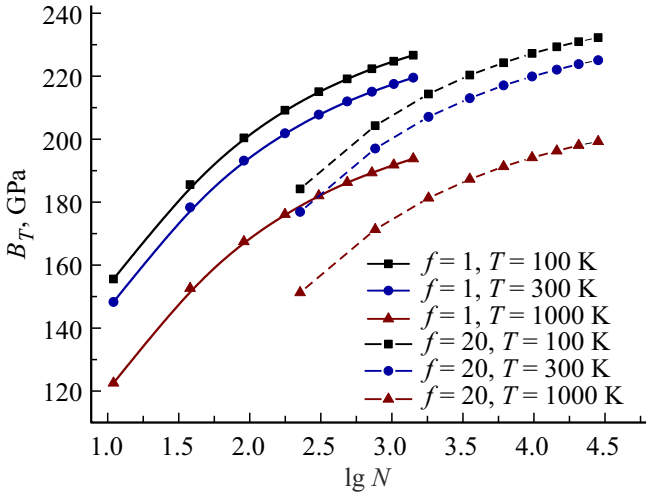

Figure 6. Isomorphic-isobaric size dependences of the compression modulus of platinum B_T ($\lg(N)$) for the three isotherms $T = 100$, 300 and 1000 K and two parameters of the shape $f = 1$ (cube) and $f = 20$ (rod) at $P = 0$.

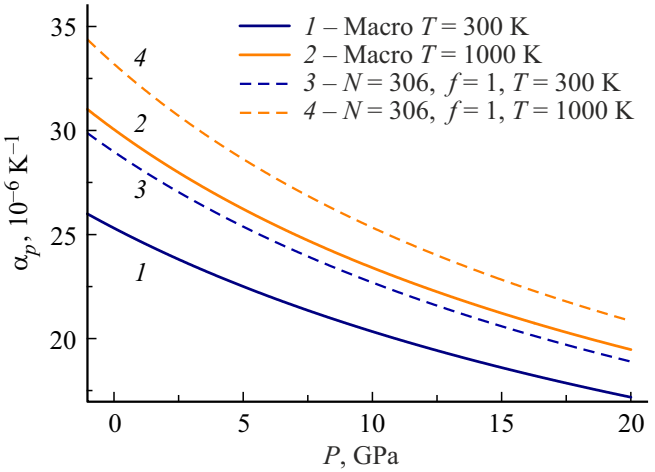

Figure 7. Baric dependences of volume thermal expansion coefficient $\alpha_p(P)$ for macro- and nanocrystals of Pt.

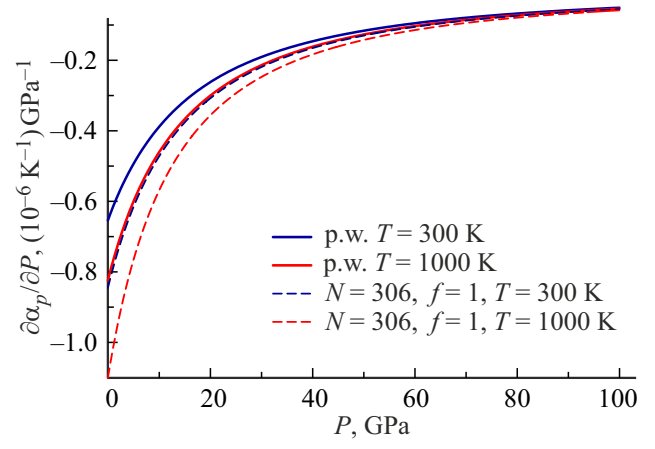

Figure 8. Baric dependence of the FCC-platinum thermal expansion coefficient derivative by pressure for two isotherms.

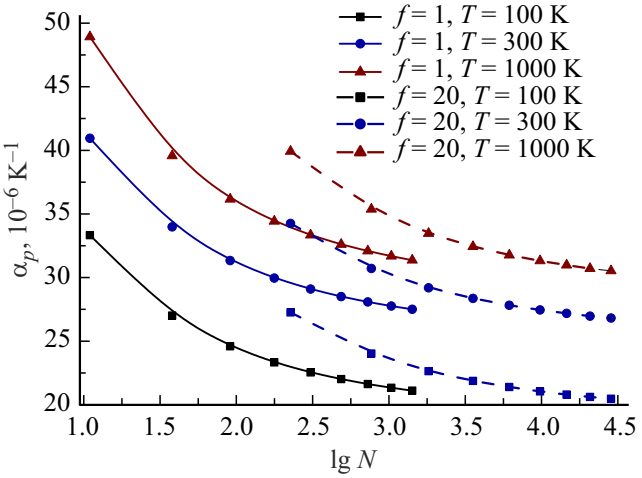

Figure 9. Isomorphic ($f = 1$ and $f = 20$) isobaric size dependences of the volume thermal expansion coefficient of platinum for three isotherms $T = 100$, 300 and 1000 K.

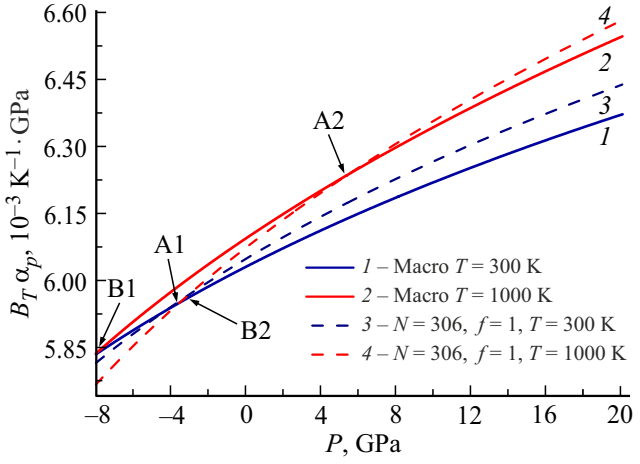

Figure 10. Baric dependences of the product $B_T\alpha_p(P)$ for FCC-Pt macro- and nanocrystal.

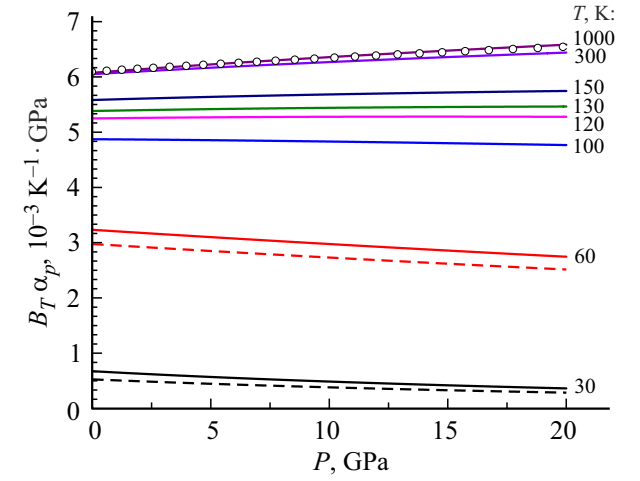

Figure 11. Baric dependences of the product $B_T\alpha_p(P)$ for FCC-Platinum macro- and nanocrystal for the wide range of temperatures.

at $N = 306$ and $f = 1$. The lines *1* and *2* are calculations for the macrocrystal along isotherms 300 and 1000 K, the lines *3* and *4* are the calculations for the nanocrystal at $N = 83$ and $f = 1$ along the isotherms $T = 300$ and 1000 K. You can see that the dependence contains points, where the product $B_T\alpha_p$ does not depend on N and on f for this temperature:
for $T = 300$ K :

$$P_{A1} = -3.75\,\text{GPa};\ B_T\alpha_p(P_{A1}) = 5.94\ [10^{-3}\,\text{K}^{-1}\,\text{GPa}],$$

for $T = 1000$ K :

$$P_{A2} = 5.29\,\text{GPa};\ B_T\alpha_p(P_{A2}) = 6.23\ [10^{-3}\,\text{K}^{-1}\,\text{GPa}].$$

There are also points where the product $B_T\alpha_p$ does not depend on temperature at this N:

$$P_{B1} = -7.98\,\text{GPa};\ B_T\alpha_p(P_{B1}) = 5.83\ [10^{-3}\,\text{K}^{-1}\,\text{GPa}]$$

for $N = \infty$,

$$P_{B2} = -3.12\,\text{GPa};\ B_T\alpha_p(P_{B2}) = 5.95\ [10^{-3}\,\text{K}^{-1}\,\text{GPa}]$$

for $N = 306$.

Evolution of the baric dependence of the product $B_T\alpha_p(P) = (\partial P/\partial T)_v$, for the macro- and nanocrystal of Pt at $N = 306$ and $f = 1$ is shown in Figure 11. For the nanocrystal of platinum FCC eight isotherms are provided in the range from T=30 to 1000 K, they are shown as solid lines in the figure. For illustration of the differences between the macro and nanocrystal for three isotherms $T = 30$, 60 and 1000 K, the dashed lines show the data for the macrocrystal. From the figure you can see that in the temperature range from $T = 120$ to 130 K the baric dependence $B_T\alpha_p(P)$, in the studied pressure range, is nearly absent, and the product $B_T\alpha_p$ may be deemed the same (for FCC Pt macro- and nanocrystals) and constant, equal to $B_T\alpha_p \approx 5.35\,[10^{-3}\,\text{K}^{-1}\,\text{GPa}]$.

Figure 12 shows the baric dependences for σ — specific (per unit of surface) surface energy of a facet (100)

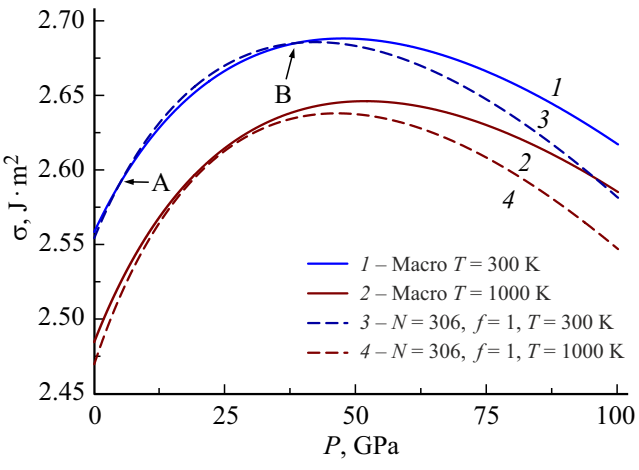

Figure 12. Baric dependences for σ — specific surface of energy of the macro- and nanocrystal of Pt.

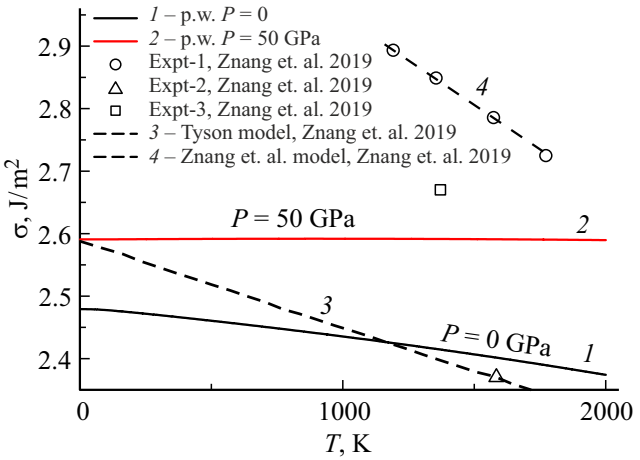

Figure 13. Temperature dependences for σ — specific surface of energy of the macrocrystal of Pt.

for the platinum macro- and nanocrystal. The lines *1* and *2* are calculations for the macrocrystal along isotherms $T = 300$ and 1000 K, the lines *3* and *4* are the calculations for the nanocrystal at $N = 306$ and $f = 1$ along the isotherms $T = 300$ and 1000 K. You can see that the baric dependences have points of maximum with the following coordinates:

$$\text{for } 300\,\text{K}: \ \sigma = 2.69\,\text{J/m}^2, \ P = 47.60\,\text{GPa}, \ \text{for } N = \infty,$$

$$\text{for } 1000\,\text{K}: \sigma = 2.64\,\text{J/m}^2, \ P = 52.34\,\text{GPa}, \ \text{for } N = \infty,$$

$$\text{for } 300\,\text{K}: \ \sigma = 2.68\,\text{J/m}^2, \ P = 41.98\,\text{GPa}, \ \text{for } N = 306,$$

$$\text{for } 1000\,\text{K}: \sigma = 2.63\,\text{J/m}^2, \ P = 46.12\,\text{GPa}, \ \text{for } N = 306.$$

The isotherm $T = 300$ K contains two specific P-points, the existence of which was noted in [23,24] using the example of iron and niobium. In P-points the value $\sigma(P)$ does not depend on N and the shape at the specified value of T. For the FCC-platinum the coordinates of P-points are the following:

$$P_\text{A} = 5.18\,\text{GPa}; \ \sigma(P_\text{A}) = 2.59\,[\text{J/m}^2],$$

$$P_\text{B} = 39.13\,\text{GPa}; \ \sigma(P_\text{B}) = 2.68\,[\text{J/m}^2].$$

For the isotherm $T = 1000$ K P-points are absent.

Figure 13 shows the temperature dependences of the specific surface energy σ of the FCC-platinum macrocrystal. The solid lines are our calculations (curves *1* and *2* isobars $P = 0$ and $P = 50$ GPa respectively), the symbols indicate experimental data: circles [25], triangle [26], square [27].

The dashed lines (curves *3* are the Tyson model and *4* — Zhang et. al.) model are the results of the calculations from paper [28]. As you can see from Figure 13, our calculations match the available experimental and calculated data. As the temperature increases, the value of the surface energy decreases in the entire range of the studied pressure values.

Further, as the pressure increases, values σ become negative, which is shown in Figure 14, *a*. The lines *1* and *2* are calculations for the macrocrystal along isotherms $T = 300$ and 1000 K, the lines *3* and *4* are the calculations for the nanocrystal at $N = 306$ and $f = 1$ along the isotherms $T = 300$ and 1000 K. At $\sigma < 0$ for the substance at these pressure values it becomes energetically favorable to increase its specific (per atom) surface, i. e. to be in the fragmented state. Below the specific points of fragmentation of Figure 14, *b* are described, where the sign σ changes:

$$P_{f1}: \ P = 627.36\,\text{GPa}, \ T = 300\,\text{K}, \ N = \infty,$$

$$P_{f2}: \ P = 625.4\,\text{GPa}, \ T = 1000\,\text{K}, \ N = \infty,$$

$$P_{f3}: \ P = 553.33\,\text{GPa}, \ T = 300\,\text{K}, \ N = 306,$$

$$P_{f4}: \ P = 551.35\,\text{GPa}, \ T = 1000\,\text{K}, \ N = 306.$$

The baric dependences of the derivative of the modulus of elasticity $(\partial\sigma/\partial P)_T$ for the FCC-Pt macro- and nanocrystal at $N = 306$ and $f = 1$ are shown in Figure 15. The solid lines are calculations for the macrocrystal along

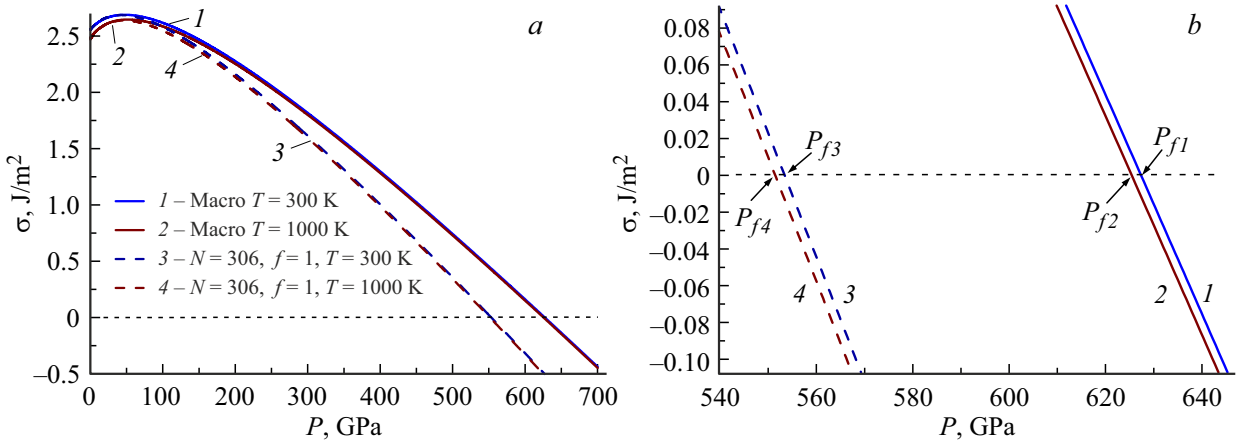

Figure 14. FCC Pt fragmentation points in dependences $\sigma(P)$ for the macro- and nanocrystal.

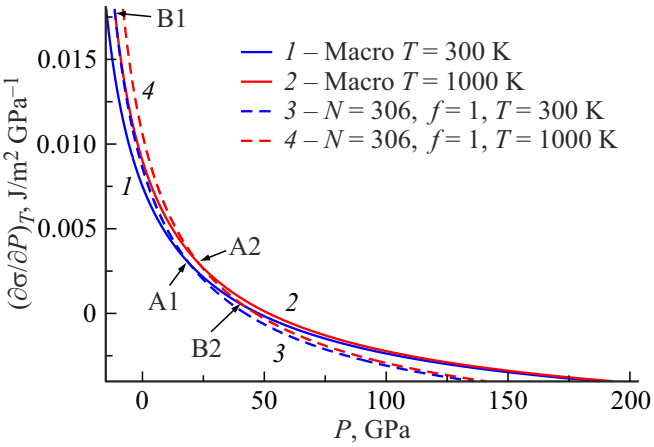

Figure 15. Baric dependences of the derivative of the specific surface energy $(\partial\sigma/\partial P)_T$ for the macro- and nanocrystal of Pt.

isotherms $T = 300$ and 1000 K, the dashed lines are the calculations for the nanocrystal at $N = 306$ and $f = 1$ along the isotherms 300 and 1000 K. You can see that the dependence contains the points with coordinates as in the case with the derivative of the modulus of elasticity $(\partial B_T/\partial P)_T$ of Figure 5:

$$P_{A1} = 18.71\,\text{GPa};\ (\partial\sigma/\partial P)_{T\,A1} = 3.02 \cdot 10^{-3}\,\text{Jm}^2\text{GPa}^{-1}$$

for $T = 300$ K,

$$P_{A2} = 22.61\,\text{GPa};\ (\partial\sigma/\partial P)_{T\,A2} = 3.04 \cdot 10^{-3}\,\text{Jm}^2\text{GPa}^{-1}$$

for $T = 1000$ K,
where $(\partial\sigma/\partial P)_T$ does not depend on N and on f for this temperature.
There are also the following points with the coordinates:

$$P_{B1} = -11.28\,\text{GPa};\ (\partial\sigma/\partial P)_{T\,B1} = 1.77 \cdot 10^{-2}\,\text{Jm}^2\text{GPa}^{-1}$$

for $N = 306$,

$$P_{B2} = -40.12\,\text{GPa};\ (\partial\sigma/\partial P)_{T\,B2} = 5.54 \cdot 10^{-4}\,\text{Jm}^2\text{GPa}^{-1}$$

for $N = \infty$,
where $(\partial\sigma/\partial P)_T$ does not depend on the temperature at this N.

Figure 16 presents isochoric (curves (*1–4*) in Figure 16, *a*) and isobaric (curves (*5–8*) in Figure 16, *b*)

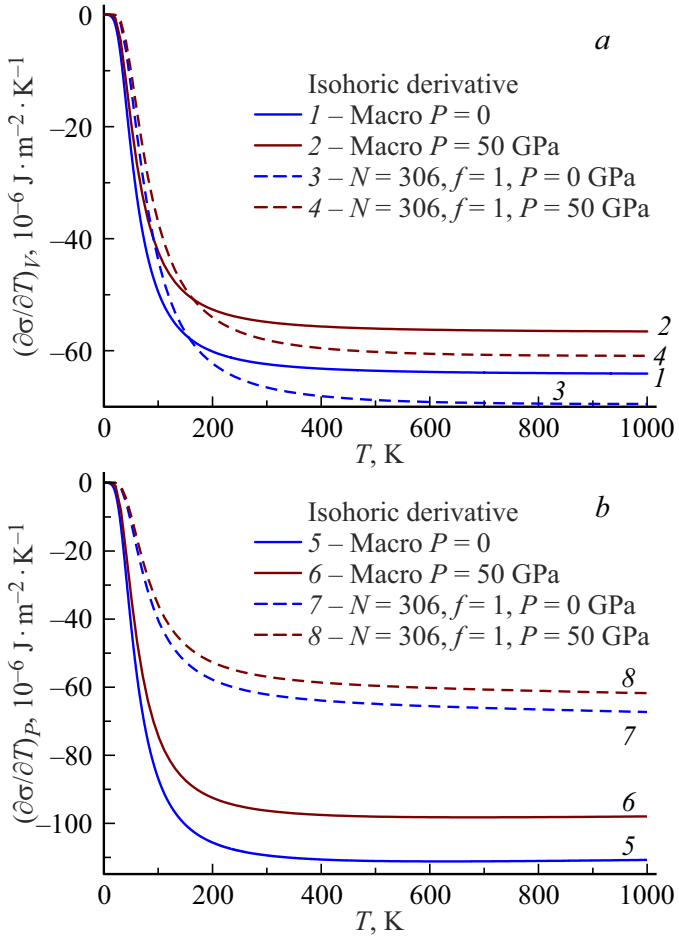

Figure 16. Isochoric and isobaric temperature dependences of the derivative of the specific surface energy $(\partial\sigma/\partial T)_{V,P}$ for the macro- and nanocrystals of Pt along two isobars $P = 0$ and $P = 50$ GPa.

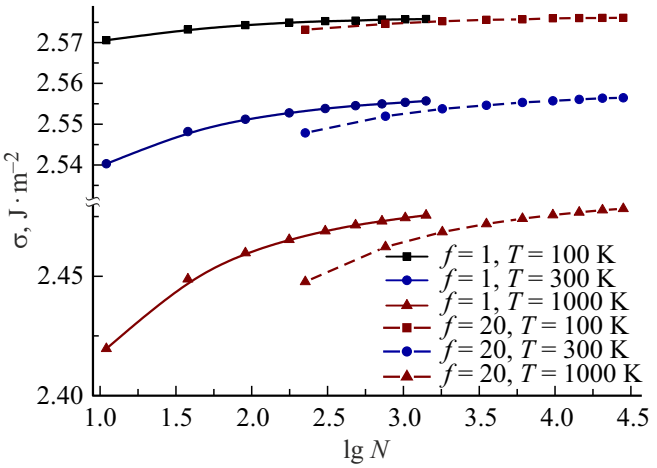

Figure 17. Isomorphic ($f = 1$ and $f = 20$) isobaric size dependences of the specific surface energy from the number of particles in the FCC-Pt nanocrystal for three isotherms $T = 100$, 300 and 1000 K.

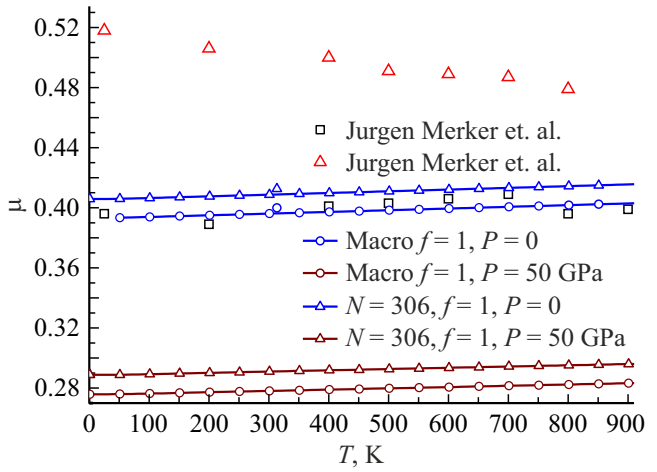

Figure 18. Isobatic temperature dependences of the Poison's ratio for the FCC-Pt macro- and nanocrystals for two pressure values $P = 0$ and $P = 50$ GPa.

temperature dependences of the derivative of the specific surface energy $(\partial\sigma/\partial T)_{V,P}$ for the macro- (curves *1, 2, 5, 6*) and nanocrystals (curves *3, 4, 7, 8*) of Pt along two isobars $P = 0$ (curves *1, 3, 5, 7*) and $P = 50$ GPa (curves *2, 4, 6, 8*). You can see that for the macrocrystal there is a huge difference in the value of the isochoric and isobaric derivatives, whereas for the nanocrystal this difference becomes minor. It should also be noted that for the isobaric derivative $(\partial\sigma/\partial T)_P$ there is a much higher difference between the values for the macro- and nanocrystals in the area of temperatures of $T > 50$ K. For all dependences you can note that there is decrease of the absolute values $(\partial\sigma/\partial T)_{V,P}$ as T increases.

In case of the isochoric dependence, as the size decreases, the absolute values $(\partial\sigma/\partial T)_V$ increase, and for the isobaric dependence there is a considerable decrease of the absolute values $(\partial\sigma/\partial T)_P$ with the decrease of the nanocrystal size.

Figure 17 shows isomorphic ($f = 1$ and $f = 20$) isobaric ($P = 0$) size dependences of $\sigma(\lg(N))$ of platinum along three isotherms. Squares, circles and triangles — isotherms $T = 100$, 300 and 1000 K, accordingly. The solid lines show the calculations for the shape parameter $f = 1$, the dashed ones — for $f = 20$. You can see that as the size decreases, the value σ decreases. You can also see that as the temperature increases, the dependence σ on the size (i.e. on N) strengthens. Both for the functions $B_t(\lg(N))$ and $\alpha_p(\lg(N))$ (Figures 6 and 9), for the dependence $\sigma(\lg(N))$ there is a stronger size dependence as the shape factor deviates more from one.

Figure 18 shows the isobaric temperature dependences of the Poison's ratio calculated using the formula [29]:

$$\mu(N, T) = \frac{1}{2} - \frac{1}{48 \cdot X_{sc}(N, T) \cdot [\gamma(N, T)]^2},$$

$$X_{sc}(N, T) = \frac{\sigma(N, T)}{c \cdot M_T(N, T)},$$

where γ — first Gruneisen parameter, σ — specific surface energy of the facet (100), B_T — modulus of elasticity. The dependences are calculated for the macro- (curves with circles) and nanocrystal of $N = 306$ atoms and $f = 1$ (curves with triangles) FCC-Pt for two pressures $P = 0$ (two middle curves with symbols) and $P = 50$ GPa (two bottom curves with symbols).

Two solid curves without symbols — literature data obtained by two different methods in paper [30]. As you can see from the figure, our dependence matches well the experimental data, and the formalism from [11,12,23,29] used in this paper makes it possible to calculate the Poison's ratio both when pressure varies and when the size of the nanocrystal decreases.

4. Conclusion

For the first time the size dependence was studied of both the equation of state and the baric dependences of the following platinum properties: isothermal modulus of elasticity, thermal expansion coefficient, product of TEC and modulus of elasticity, specific surface energy and Poison's ratio. Besides, the derivatives of these functions by pressure and temperature were also studied.

The specific points where the isotherms of the equation of state of the macro- and nanocrystals intersect with the coordinates are found in Figure 3:

$$P_A = 1.87\,\text{GPa}, \quad (v/v_o)_A = 1.0003, \quad T = 300\,\text{K};$$

$$P_B = 6.16\,\text{GPa}, \quad (v/v_o)_B = 1.0005, \quad T = 1000\,\text{K}.$$

In these points the pressure does not depend on the size (N) at this temperature and shape of the nanocrystal.

When the baric dependence $B_T\alpha_p(P)$ was studied (Figure 11) it was found that in the temperature range

from $T = 120$ to 130 K the baric dependence $B_T\alpha_p(P)$, in the studied pressure range, is nearly absent, and the product of $B_T\alpha_p$ may be deemed to be the same (for the FCC Pt macro- and nanocrystals) and constant, equal to $B_T\alpha_p \approx 5.35\,[10^{-3}\,\mathrm{K}^{-1}\mathrm{GPa}]$, this statement matches the Birch's assumption [31] on the constancy of the product of $B_T\alpha_p$, however, this statement is true in the narrow temperature range, which you can see well in Figure 11.

It is shown that as the size decreases, α_p values increase, and B_T decrease along the isobar. For σ there is a more complicated dependence pattern, but at pressure of $P > 39.13$ GPa the trend towards the decrease of σ value with the size decrease remains for isotherm 300 K. For isotherm 1000 K the σ values decrease with the isomorphic decrease of the size along the isobar. As the shape deviates from the energetically optimal one, i. e. from the cube ($f = 1$), the size dependences for the studied functions become more evident. This statement is illustrated using the example of the size dependences of the functions $B_t(N)$, $\alpha_p(N)$ and $\sigma(N)$ for the three isotherms in Figures 6, 9 and 17, respectively. The specified behavior of the size dependences of the thermoelastic properties was studied for the tungsten nanocrystals in paper [22].

It was also shown that the baric dependence $\sigma(P)$ contains the points where the maximum surface energy is observed:

$$\text{for } 300\,\mathrm{K}\ \sigma = 2.69\,\mathrm{J/m^2},\ P = 47.60\,\mathrm{GPa},\ \text{for } N = \infty,$$

$$\text{for } 1000\,\mathrm{K}\ \sigma = 2.64\,\mathrm{J/m^2},\ P = 52.34\,\mathrm{GPa},\ \text{for } N = \infty,$$

$$\text{for } 300\,\mathrm{K}\ \sigma = 2.68\,\mathrm{J/m^2},\ P = 41.98\,\mathrm{GPa},\ \text{for } N = 306,$$

$$\text{for } 1000\,\mathrm{K}\ \sigma = 2.63\,\mathrm{J/m^2},\ P = 46.12\,\mathrm{GPa},\ \text{for } N = 306,$$

besides, P-points are also observed in this dependence. In P-points the value $\sigma(P)$ does not depend o N and the shape at the specified value of T. For the isotherm $T = 1000$ K P-points are absent. We obtained the following coordinates of P-points (isotherm $T = 300$ K):

$$P_\mathrm{A} = 5.18\,\mathrm{GPa};\ \sigma(P_\mathrm{A}) = 2.59\,[\mathrm{J/m^2}],$$

$$P_\mathrm{B} = 39.13\,\mathrm{GPa};\ \sigma(P_\mathrm{B}) = 2.68\,[\mathrm{J/m^2}].$$

As the pressure increases further, the values $\sigma(P)$ continue decreasing and then become negative, which is illustrated in Figure 14. At $\sigma < 0$ for the substance it becomes energetically favorable to increase its specific (per atom) surface, i. e. transition to the fragmented state. The following values of the fragmentation points were obtained for the FCC-Pt macro- and nanocrystals, where the sign σ changes:

$$P_{f1}:\ P = 627.36\,\mathrm{GPa},\ T = 300\,\mathrm{K},\ N = \infty,$$

$$P_{f2}:\ P = 625.4\,\mathrm{GPa},\ T = 1000\,\mathrm{K},\ N = \infty,$$

$$P_{f3}:\ P = 553.33\,\mathrm{GPa},\ T = 300\,\mathrm{K},\ N = 306,$$

$$P_{f4}:\ P = 551.35\,\mathrm{GPa},\ T = 1000\,\mathrm{K},\ N = 306.$$

When temperature dependences $(\partial\sigma/\partial T)$ were studied, it was found that in case of the isochoric dependence, as the size decreases, the absolute values $(\partial\sigma/\partial T)_V$ increase, and for the isobaric dependence there is a considerable decrease of the absolute values $(\partial\sigma/\partial T)_P$ with the decrease of the nanocrystal size.

For the first time the evolution of the temperature dependence of the Poison's ratio was studied with the decrease of the size along two isobars $P = 0$ and $P = 50$ GPa. It is shown that as the size of the nanocrystal decreases, the increase of μ occurs in the entire range of the temperatures and pressures. Pressure increase results in significant decrease of μ, since pressure increase to 50 GPa causes $\mu_{P=0}/\mu_{P=50\,\mathrm{GPa}} \approx 1.42$ fold decrease of μ.

Acknowledgments

The author expresses gratitude to M.N. Magomedov and N.L. Kramynina for the fruitful discussions and assistance.

Funding

This study was supported by the Russian Science Foundation, grant No. 25-23-00001, https://rscf.ru/project/25-23-00001/.

Conflict of interest

The authors declare that they have no conflict of interest.

References

[1] S. Zhang, X. He, Y. Ding, Z. Shi, B. Wu. Renew. Sust. Energ. Rev. **204**, 114821 (2024). DOI: 10.1016/j.rser.2024.114821
[2] T. Sakai, H. Kadobayashi, Y. Nakamoto, H. Dekura, N. Ishimatsu1, S. Kawaguchi-Imada, Y. Seto, O. Sekizawa, K. Nitta, K. Shimizu. Commun. Mater. **6**, 68 (2025). DOI: 10.1038/s43246-025-00792-5
[3] Z. Li, L. Hao, X. Wang, G. Li, Y. Hou, Q. Wang, L. Liu, H. Geng, Y. Yu, C. Dai, Q. Wu, J. Hu. Phys. Rev. B **109**, 144109 (2024). DOI: 10.1103/PhysRevB.109.144109
[4] P.I. Dorogokupets, A.R. Oganov. Phys. Rev. B **75**, 024115 (2007). DOI: 10.1103/PhysRevB.75.024115
[5] C. Zha, K. Mibe, W.A. Bassett, O. Tschauner, H. Mao, R.J. Hemley. J. Appl. Phys. **103**, 054908 (2008). DOI: 10.1063/1.2844358
[6] N. Tian, Z. Zhou, S. Sun, Y. Ding, Z. Lin Wang. Science **316**, 732 (2007). DOI: 10.1126/science.1140484
[7] X. Yin, M. Shi, J. Wu, Y.T. Pan, D.L. Gray, J.A. Bertke, H. Yang. Nano Lett. **17**, 6146 (2017). DOI: 10.1021/acs.nanolett.7b02751
[8] W. Dachraoui, T.R. Henninen, D. Keller, R. Erni. Sci. Rep. **11**, 23965 (2021). DOI: 10.1038/s41598-021-03455-w
[9] Y. Xia, D. Nelli, R. Ferrando, J. Yuan, Z.Y. Li. Nature Commun. **12**, 3019 (2021). DOI: 10.1038/s41467-021-23305-7
[10] M.I. Richard, S. Labat, M. Dupraz, J. Carnis, L. Gao, M. Texier, N. Li, L. Wu, J. Hofmann, M. Levi, S.J. Leake, S. Lazarev, M. Sprung, E.J.M. Hensen, E. Rabkin, O. Thomas. ACS Nano **17**, *6*, 6113–6120 (2023). DOI: 10.1021/acsnano.3c01306.hal-04033846

[11] M.N. Magomedov. Phys. Solid State **63**, *10*, 1465 (2021). DOI: 10.1134/S1063783421090250
[12] M.N. Magomedov. J. Phys. Chem. Sol. **151**, 109905 (2021). DOI: 10.1038/s41467-021-23305-7
[13] D.E. Fratanduono, M. Millot, D.G. Braun, S.J. Ali, A. Fernandez-Pañella, C.T. Seagle, J.-P. Davis, J.L. Brown, Y. Akahama, R.G. Kraus, M.C. Marshall, R.F. Smith, E.F. O'Bannon III, J.M. McNaney, J.H. Eggert. Science **372**, 1063 (2021). DOI: 10.1126/science.abh0364
[14] J.L. Brown, J.P. Davis, J.D. Tucker, G. Huerta, K.W. Shuler. J. Appl. Phys. **134**, *23*, 235902 (2023). DOI: 10.1063/5.0173652
[15] J.P. Davis, J.L. Brown. J. Appl. Phys. **134**, *23*, 235901 (2023). DOI: 10.1063/5.0173534
[16] X. Huang, F. Li, Q. Zhou, G. Wu, Y. Huang, L. Wang, B. Liu, T. Cui. RSC Advances **5**, 14603 (2015). DOI: 10.1039/c4ra12769b
[17] S. Ono, J.P. Brodholt, G.D. Price. J. Phys. Chem. Sol. **72**, *3*, 169 (2011). DOI: 10.1016/j.jpcs.2010.12.004
[18] A. Dewaele, P. Loubeyre, M. Mezouar. Phys. Rev. B **70**, 094112 (2004). DOI: 10.1103/PhysRevB.70.094112
[19] M. Yokoo, N. Kawai, K.G. Nakamura, K. Kondo. Phys. Rev. B **80**, 104114 (2009). DOI: 10.1103/PhysRevB.80.104114
[20] J W. Arblaster. Platinum Metals Review. **41**, *1*, 12 (1997).
[21] Y. Fei, J. Li, K. Hirose, W. Minarik, J.V. Orman, C. Sanloup, W. Westrenen, T. Komabayashi, K. Funakoshi. Phys. Earth Planet. Inter. **143**−**144**, 515 (2004). DOI: 10.1016/j.pepi.2003.09.018
[22] S.P. Kramynin. J. Phys. Chem. Sol. **152**, 09964 (2021). DOI: 10.1016/j.jpcs.2021.109964
[23] M.N. Magomedov. Phys. Solid State **66**, *10*, 1569 (2024). DOI: 10.61011/PSS.2024.10.59615.151
[24] S.P. Kramynin. J. Phys. Chem. Sol. **143**, 109464 (2020). DOI: 10.1016/j.jpcs.2020.109464
[25] M. McLean, H. Mykura. Surf. Sci. **5**, *4*, 466 (1966). DOI: 10.1016/0039-6028(66)90042-2
[26] M. McLean, E.D. Hondros. J. Mater. Sci. **6**, 19 (1971). DOI: 10.1007/BF00550286
[27] S.K. Rhee. Mater. Sci. Eng. **16**, *1*−*2*, 45 (1974). DOI: 10.1016/0025-5416(74)90136-0
[28] X. Zhang, W. Li, H. Kou, J. Shao, Y. Deng, X. Zhang, J. Ma, Y. Li, X. Zhang. J. Appl. Phys. **125**, 185105 (2019). DOI: 10.1063/1.5090301
[29] M.N. Magomedov. J. Surf. Investig.: X-ray, Synchrotron Neutron Tech. **12**, *1*, 185−196 (2018). DOI: 10.1134/S1027451018010299
[30] J. Merker, D. Lupton, M. Töpfer, H. Knake. Platin. Met. Rev. **45**, *2*, 74 (2001).
[31] M.N. Magomedov. Comput. Condens. Matter **31**, e00673 (2022). DOI: 10.1016/j.cocom.2022.e00673

Translated by M.Verenikina